COUPLING BETWEEN ELECTROMAGNETIC AND MECHANICAL VIBRATIONS OF THIN-WALLED STRUCTURES

by S. GUENNEAU

(*The Blackett Laboratory, Imperial College, London* SW7 2EZ)

A. B. MOVCHAN

(*Department of Mathematical Sciences, University of Liverpool, Liverpool* L69 3BX)

C. G. POULTON

(*High-Frequency and Quantum Electronics Laboratory, Institut für Höchfrequenztechnik und Quanten Elektronik, Universität Karlsruhe, Gebäude* 30.10, *Engesserstrasse* 5, D-76131 *Karlsruhe, Germany*)

and A. NICOLET

(*Institut Fresnel, UMR* 6133, *Faculté de St Jérôme, case* 162, F-13397 *Marseille Cedex* 20, *France*)

[Received 13 October 2003. Revise 18 March 2004]

Summary

The paper addresses the issue of coupling between the electromagnetic and elastic vibrations and deals with the following three classes of problems: vibration of thin bodies in an electromagnetic field; a coupling that occurs due to perturbation of boundaries within a deformed solid; and a coupling within regions of localized stress in a composite structure with defects. It is shown that the coupling effect is negligibly small in the first case, while it becomes important in the last two classes of problems. For vibrations of thin-walled conducting solids placed in an electromagnetic field we present a systematic new asymptotic scheme. It is observed that the magnetic field induces a 'viscous force', which is similar to certain problems that occur in magnetic fluids flows. When we deal with electromagnetic waves propagating through a thin-walled periodic structure subject to regular perturbation of the boundary, an asymptotic method is applied to derive the effective boundary conditions for the perturbed inclusion within the array. We examine the effect of this perturbation on the dispersion curves for the corresponding spectral problem, and compare the asymptotic results with a finite element modelling of the perturbed structure. Finally, we show exciting results describing coupling between electromagnetic and elastic fields due to the localization associated with a defect mode in a doubly periodic structure.

1. Introduction

It is known and well described in the classical literature that there is a coupling between electromagnetic and elastic signals in elastic media. The famous example is Brillouin scattering,

predicted in 1922 (**1**) and supported by experimental studies by Debye and Sears (**2**) in 1932. The purpose of this paper is to analyse asymptotic models for isotropic media, where the coupling between electromagnetic and elastic waves occurs, and to give appropriate classification. The domains considered here are composite structures involving arrays of closely packed voids or model thin-walled structures. This analytical study is motivated by important physical applications associated with the design of photonic crystal fibres and described in the recent paper (**3**).

The classical sources describing the interaction between light and sound include monographs (**4** to **6**), articles (**7**,**8**) and the recent monograph by Wolfe (**9**). These effects are extremely important in the theory of photonic crystal fibres, as was confirmed by the studies (**10** to **12**).

Our structures have a common feature: they all contain thin elastic ligaments separating inclusions/voids, and hence it seems natural to apply an asymptotic method to analyse coupled fields within such domains. In this study we aim to conduct a comparative analysis of thin-walled structures of different types and select the one where the coupling effects are most pronounced. It will be shown in the text below that the defect modes associated with the highly localized strain are the ones that bring the interesting and new effects. We consider three possible cases of coupling: via the governing equations that involve the Lorentz force for an elastic conductor moving in the electromagnetic field; via the boundary conditions posed on the boundary perturbed due to elastic vibrations; and finally due to localization associated with the presence of the so-called defect modes in composite structures. It will be shown that the last class (defect modes) dominates over the two other types of coupling between elastic and electromagnetic waves.

The paper is organized as follows. We begin with the analysis of the model of a thin elastic domain subject to time-harmonic motion in a constant magnetic field. An asymptotic approximation shows that the transverse component of the magnetic field produces a ‘viscous force’ that would supress longitudinal vibrations of the thin body. The conclusions of this section are consistent with the analysis given by Maugin in (**13**, Chapter 5). It is also shown that the coupling effect is rather small and becomes important only within the relativistic range of velocities. Despite the fact that this physical effect is well known, the asymptotic procedure used to derive the lower-dimensional model is original, and is included in Appendix A.

In section 3, we consider a thin-walled periodic structure whose boundaries are slightly perturbed, due to an elastic deformation, for example. The motivation for this model comes from consideration of an elastic composite structure vibrating in an electromagnetic field. Since the typical frequencies of elastic and electromagnetic waves are of different orders of magnitude, one can take a ‘snap shot’ of the deformed structure and analyse the corresponding spectral problem for equations of electromagnetism. Assuming that the unperturbed structure consists of a doubly periodic array of circular voids, we introduce a new perturbation problem where the contour of the void in an elementary cell is regularly perturbed. We develop an asymptotic algorithm that produces a correction of frequencies and analyse the dispersion diagrams. The results of the asymptotic analysis are compared with the numerical test produced independently via the finite element algorithm.

Finally, in section 4 we again consider a thin-walled structure consisting of an infinite array of circular voids, but on this occasion we introduce an array of periodically distributed defects. Of course, the corresponding spectral problem will have new features, and in particular it exhibits localized defect modes discussed in the main text of the paper. We speak about photoelastic effects and interaction between electromagnetic and elastic waves associated with localization. In addition to the key concept and numerical illustrations, we also propose a simple analytical formula which provides an approximation for the frequency corresponding to the localized dilatational

defect modes. We conclude by giving examples of multiple localization effects that can be used in modelling optical switches and can stimulate further research.

2. Elastic displacements and electromagnetic fields within a thin domain

In the present section we analyse the problem of coupling between magnetic and elastic fields within a thin conducting body. The asymptotic procedure used here has certain features in common with the lubrication approximations for magnetic fluids.

2.1 *Governing equations*

Let us consider electromagnetic fields $(\mathbf{E}, \mathbf{H})$ and a thin domain

$$\Pi_\varepsilon = \{(x_1, x_2) : |x_1| < \tfrac{1}{2}, |x_2| < \varepsilon/2\}, \tag{2.1}$$

where ε is a small non-dimensional parameter. Typically, it is common to use a characteristic length l and width h and take the small parameter as the aspect ratio $\varepsilon = h/l$; here we certainly follow this pattern but for the sake of simplifying the notation we introduce the normalization in such a way that $l = 1$ and $h = \varepsilon$. The electric and magnetic fields $\mathbf{E}$ and $\mathbf{H}$ are divergence free,

$$\nabla \cdot \mathbf{E} = 0 \quad \text{and} \quad \nabla \cdot \mathbf{H} = 0, \tag{2.2}$$

and satisfy the system of Maxwell's equations

$$\nabla \times \mathbf{H} - \frac{1}{c}\frac{\partial \mathbf{D}}{\partial t} = \mathbf{J}, \quad \nabla \times \mathbf{E} + \frac{\mu_0}{c}\frac{\partial \mathbf{H}}{\partial t} = \mathbf{0},$$

where $\mathbf{D}$ is the electric displacement. We consider the vibrations of the thin body Π_ε characterized by a displacement field $\mathbf{u}$, which satisfies the equation of motion

$$\mu \nabla^2 \mathbf{u} + (\lambda + \mu)\nabla(\nabla \cdot \mathbf{u}) + \mu_0(\mathbf{J} \times \mathbf{H}) = \rho \ddot{\mathbf{u}}, \tag{2.3}$$

where λ and μ are the Lamé elastic moduli, μ_0 is the permeability of the material in Π_ε and c is the speed of light. Also, the electric current density $\mathbf{J}$ is related to $\mathbf{E}$, $\mathbf{H}$ and $\mathbf{u}$ by Ohm's law:

$$\mathbf{J} = \sigma\{\mathbf{E} + \mu_0 \dot{\mathbf{u}} \times \mathbf{H}\}, \tag{2.4}$$

where σ is the electric conductivity of the thin body.

The initial boundary-value problem. Taking the curl in the first Maxwell's equation

$$c\nabla \times (\nabla \times \mathbf{H}) - \nabla \times \dot{\mathbf{D}} = c\nabla \times \mathbf{J}$$

and applying Ohm's law (2.4) in the second Maxwell's equation we obtain

$$c\nabla \times (\nabla \times \mathbf{H}) - \nabla \times \dot{\mathbf{D}} = \mu_0\sigma\{-\dot{\mathbf{H}} + \nabla \times (\dot{\mathbf{u}} \times \mathbf{H})\}.$$

Since $\mathbf{H}$ is divergence free, $\nabla \times (\nabla \times \mathbf{H}) = -\nabla^2 \mathbf{H}$. Therefore

$$-\nabla^2 \mathbf{H} = c^{-1}\nabla \times \dot{\mathbf{D}} + \mu_0\sigma\{-\dot{\mathbf{H}} + \nabla \times (\dot{\mathbf{u}} \times \mathbf{H})\}. \tag{2.5}$$

Taking into account (2.4), we represent the equation of motion (2.3) in the form

$$\mu\nabla^2\mathbf{u} + (\lambda+\mu)\nabla(\nabla\cdot\mathbf{u}) + \mu_0\sigma\mathbf{E}\times\mathbf{H} + \mu_0^2\sigma(\dot{\mathbf{u}}\times\mathbf{H})\times\mathbf{H} = \rho\ddot{\mathbf{u}}. \tag{2.6}$$

Hence, **E**, **H** and **u** satisfy (2.2), (2.5) and (2.6) in Π_ε. It is assumed that in the exterior of Π_ε there exists a constant electromagnetic field

$$\mathbf{E}^{(e)} = (E_1^{(e)}, E_2^{(e)}), \quad \mathbf{H}^{(e)} = (H_1^{(e)}, H_2^{(e)}). \tag{2.7}$$

The boundary conditions are set as

$$\mathbf{E}|_{\partial\Pi_\varepsilon} = \mathbf{E}^{(e)}, \quad \mathbf{H}|_{\partial\Pi_\varepsilon} = \mathbf{H}^{(e)} \tag{2.8}$$

and

$$\sigma_{ij}(\mathbf{u})n_j|_{\partial\Pi_\varepsilon} = 0, \quad j \text{ is the index of summation,} \tag{2.9}$$

where n_j are components of the unit outward normal, $\sigma_{ij} = \mu(\partial u_i/\partial x_j + \partial u_j/\partial x_i) + \lambda\delta_{ij}\nabla\cdot\mathbf{u}$. The system is supplied with appropriate initial conditions; for example, we can assume that the inital displacement and velocity fields are specified.

2.2 *Longitudinal elastic vibrations in a transverse magnetic field*

The asymptotic algorithm outlined in Appendix A shows a sequence of auxiliary model problems on the scaled cross-section of the thin body. In particular, the solvability conditions of the problem (A.9), (A.10) give a lower-dimensional model involving x_1 and t derivatives of the leading-order approximation $\mathbf{u}^{(0)}(x_1, t)$ of the displacement field. The illustration is then related to a particular simple example when the 'thin beam' vibrates along the x_1-axis, and the ambient magnetic field is parallel to the x_2-axis. In this case the longitudinal and transverse displacement modes in (A.9), (A.10) decouple, and one can set $u_2^{(0)} = 0$. Also, we have $\mathbf{H}^{(0)} = H_2^{(0)}\mathbf{e}^{(2)}$ and $\mathbf{E}^{(0)} = E_2^{(0)}\mathbf{e}^{(2)}$ as given vector functions. The boundary-value problem (A.9), (A.10) for $u_1^{(2)}$ is solvable, provided

$$\frac{E}{1-\nu^2}\frac{\partial^2 u_1^{(0)}}{\partial x_1^2} - \rho\ddot{u}_1^{(0)} + \mu_0^2\sigma\dot{u}_1^{(0)}(H_2^{(0)})^2 = 0, \tag{2.10}$$

where E is the Young's modulus, ρ the density, σ the conductivity, and ν is the Poisson ratio of the thin elastic body. When $\sigma = 0$, (2.10) becomes the wave equation, as expected. On the other hand, in the presence of a transverse magnetic field the equation contains the 'viscous force' term and the elastic vibrations in the conducting beam attenuate.

We would like to refer to the lubrication type algorithms that were used in magneto-hydrodynamics; see (**14**, Chapter 8). In this case the magnetic field will also produce a viscous force which will flatten the velocity profile for a magnetic fluid flow in a channel. The model problem associated with this effect is known in the literature as the Hartmann flow problem; see (**15**, Chapter 4). Similar models describing coupling of elastic and electromagnetic fields were discussed in (**13**). In particular, it is important to mention that the 'viscous force' term in (2.10) is very small. It becomes significant only for fairly large values of the velocity or a large magnitude of the exterior magnetic field: $\mu_0 = 4\pi \times 10^{-7}\,\mathrm{N\,A^{-2}}$ and the typical value of electrical conductivity for silver

is $\sigma = 0{\cdot}62 \times 10^8 \mathrm{A}^2\mathrm{s}^3\mathrm{m}^{-3}\mathrm{kg}^{-1}$, which implies that $\mu_0^2\sigma = 9{\cdot}791 \times 10^{-5}\mathrm{N\,s\,A}^{-2}\mathrm{m}^{-2}$. This coefficient is indeed much smaller than the coefficients near the second-order derivatives of $u_1^{(0)}$ in (2.10). On the other hand, one may think of high-magnetic-field Tokamak experiments described in (**16**): in this particular case, the 'viscous force' term in (2.10) becomes important.

In addition to the above analysis, one can think about a perturbation of the boundary of a thin body due to an elastic deformation, and this may also bring a contribution towards the electromagnetic fields. This effect may be amplified even further if we consider an infinite array (a network) of thin ligaments associated with a doubly periodic array of closely located voids. In the following section, we shall consider such a perturbation problem, which outlines more pronounced coupling between elastic and electromagnetic fields through a regular perturbation of boundary conditions within a composite structure.

3. A perturbation problem for an array of quasi-circular inclusions

In this section we show that a regular perturbation of the boundary is associated with the change of eigenvalues for a certain spectral problem. The model considered in this section involves a scalar spectral problem for the Helmholtz operator. In this particular case, we can think of a regular perturbation associated with a deformation of an elastic body, and the perturbed geometry shows a 'snap shot' of a vibrating elastic structure. We use the fact that the ranges of frequencies for elastic and electromagnetic waves are very different: the electromagnetic frequencies are much higher compared with those in the acoustic range. The spectral problem considered here is associated with the transverse electromagnetic field (TE polarization). The asymptotic analysis given below yields an explicit analytical formula for the new perturbed eigenfrequencies.

3.1 *A spectral problem*

We consider a doubly periodic array of cylindrical inclusions; C denotes the boundary of the crosss-section of a single cylinder, which is not necessarily circular. A transverse time-harmonic electromagnetic wave propagating through this material can be represented by a scalar function $u(r, \theta)$, which obeys the Helmholtz equation in the exterior of inclusions

$$(\nabla^2 + k^2)u = 0, \tag{3.1}$$

where $k = \omega/c$ is the spectral parameter, with ω, c being the radian frequency and the wave speed, respectively. On the boundary of the elementary cell, the function u satisfies the Bloch–Floquet condition (see (**5**))

$$u(\mathbf{x} + \mathbf{d}) = u(\mathbf{x})\ \exp(i\mathbf{k}_{\mathrm{Bloch}} \cdot \mathbf{d}), \tag{3.2}$$

where $\mathbf{x} = (r, \theta)$ and $\mathbf{d}$ is any vector that can be drawn from the centre of one elementary cell to the centre of another cell within the array. The vector $\mathbf{k}_{\mathrm{Bloch}}$ is commonly known as the Bloch vector. We assume that on the boundary C of the inclusions

$$\partial u/\partial n|_{\partial C} = 0; \tag{3.3}$$

for a TE polarization, this corresponds to perfectly conducting inclusions. The relationship between k and $\mathbf{k}_{\mathrm{Bloch}}$ is known as the dispersion relation for the array. The choice of perfectly conducting inclusions is made for the sake of simplicity. The asymptotic algorithm, presented below, allows

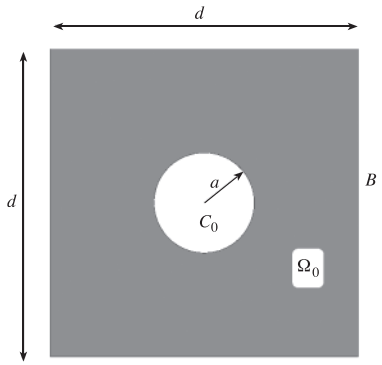

Fig. 1 The geometry for the unperturbed problem

for a straightforward generalization to the case of dielectric inclusions with transmission conditions prescribed at their boundaries.

Given $\mathbf{k}_{\text{Bloch}}$ one can determine ω and u for a fixed geometry. However, if the boundary ∂C is perturbed we shall see the change in the eigenfrequencies. This section gives analytical estimates for such small perturbations.

3.2 *Unperturbed model problem*

We begin with a single, unperturbed, cell of the array, as shown in Fig. 1, and consider the exterior region Ω_0, with a boundary $\partial C_0 \cup B$, where $C_0 = \{(r, \theta) : r \leqslant a\}$ is the circular region which corresponds to the body of the central inclusion, and B is the outer boundary of the central unit cell. Within Ω_0 we introduce the unperturbed field $u_0(r, \theta)$, which satisfies

$$(\nabla^2 + k_0^2)u_0 = 0, \tag{3.4}$$

where k_0 is the unperturbed spectral parameter. On the boundary of the inclusion we specify (as in (3.3)) a homogeneous Neumann condition, $\partial u_0/\partial n|_{\partial C_0} = 0$. As mentioned above, the periodicity of the problem requires that the Bloch–Floquet condition be satisfied throughout the unit cell: u_0 satisfies (3.2). The solution u_0 can be normalized with

$$\int_{\Omega_0} |u_0|^2 dA = 1. \tag{3.5}$$

We now note that this problem for circular cylinders is very well studied, and there are at least three different methods available by which the solution can be constructed. These methods are known as plane wave, multipole and transfer matrix methods (**17** to **19**).

3.3 *Perturbation of the boundary*

We now perturb the boundary, so that $\partial C_0 \to \partial C_1$. The new boundary of the inclusion can be described by the curve

$$r = a + \varepsilon h(\theta), \tag{3.6}$$

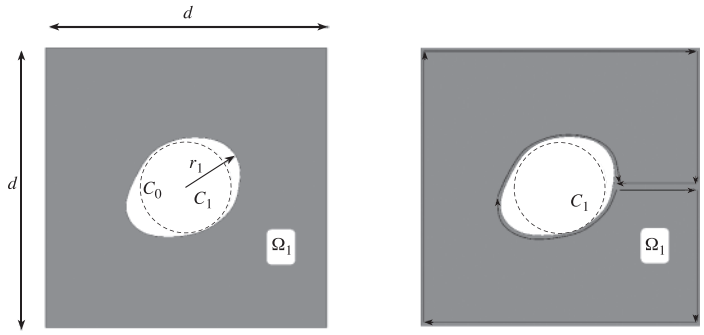

Fig. 2 Left: the geometry for the perturbed problem. The dashed line shows the unperturbed circular boundary. Right: the contour to be used for the application of Green's theorem

where $h(\theta)$ is a smooth function and ε is a small parameter such that $\varepsilon h(\theta) \ll a$. The region of the perturbed inclusion is $C_1 = \{(r, \theta) : r \leqslant a + \varepsilon h(\theta)\}$ and the region Ω_1 is the remaining region within the unit cell. Without loss of generality, we specify that $h(\theta) \geqslant 0$, so that the unperturbed inclusion C_0 lies entirely within C_1; see Fig. 2.

The solution to the perturbed problem is denoted by u_1, and it satisfies

$$(\nabla^2 + k_1^2)u_1 = 0, \tag{3.7}$$

with the boundary condition

$$\partial u_1/\partial n|_{\partial C_1} = 0. \tag{3.8}$$

The function u_1 also satisfies the Bloch–Floquet condition (3.2).

3.4 *First-order correction for the eigenvalues*

We would like to examine the effect of the perturbation of the boundary on the spectral parameter k_0. To do this, we apply Green's theorem within the region Ω_1, using the perturbed field u_1 and a function which is the complex conjugate of u_0, which we designate $\overline{u}_0$. Using the contour depicted in Fig. 2, we obtain

$$\int_{\Omega_1} (\overline{u}_0 \Delta u_1 - u_1 \Delta \overline{u}_0)\, dA = \int_{\partial C_1 \cup B} \left(u_1 \frac{\partial \overline{u}_0}{\partial n} - \overline{u}_0 \frac{\partial u_1}{\partial n} \right) d\ell. \tag{3.9}$$

We now take into account the fact that the function $\overline{u}_0$ satisfies a conjugate quasiperiodicity condition to (3.2), $\overline{u}_0(\mathbf{x} + \mathbf{d}) = \overline{u}_0(\mathbf{x}) \exp(-i\mathbf{k}_{\text{Bloch}} \cdot \mathbf{d})$. This causes the integral around the outer boundary B to be zero in (3.9). In addition, we know that $\overline{u}_0$ and u_1 satisfy (3.4) and (3.7), respectively, and so we deduce that

$$(-k_1^2 + k_0^2) \int_{\Omega_1} u_1 \overline{u}_0\, dA = \int_{\partial C_1} \left(u_1 \frac{\partial \overline{u}_0}{\partial n} - \overline{u}_0 \frac{\partial u_1}{\partial n} \right) d\ell. \tag{3.10}$$

The problem is regularly perturbed, and hence the field will behave 'reasonably' in response to the smooth perturbation of the boundary (**20**, **21**). Specifically,

$$u_1 = u_0 + \mathcal{O}(\varepsilon) \quad \text{and} \quad \frac{\partial u_1}{\partial n} = \frac{\partial u_0}{\partial n} + \mathcal{O}(\varepsilon) \quad \text{in } \Omega_1. \tag{3.11}$$

In this case the eigenvalues will also behave reasonably, and we can write $k_1 = k_0 + \delta k$, where δk is $\mathcal{O}(\varepsilon)$. With this in mind, we can write (3.10) as

$$-2k_0\delta k \int_{\Omega_1} |u_0|^2 \, dA = \int_{\partial C_1} \left(u_1 \frac{\partial \overline{u}_0}{\partial n} - \overline{u}_0 \frac{\partial u_1}{\partial n} \right) d\ell + \mathcal{O}(\varepsilon^2).$$

Thanks to (3.5) and (3.11), we also know that

$$\int_{\Omega_1} |u_0|^2 \, dA = \int_{\Omega_0} |u_0|^2 \, dA + \mathcal{O}(\varepsilon) = 1 + \mathcal{O}(\varepsilon),$$

and hence

$$\begin{aligned} \delta k &= -\frac{1}{2k_0} \int_{\partial C_1} \left(u_1 \frac{\partial \overline{u}_0}{\partial n} - \overline{u}_0 \frac{\partial u_1}{\partial n} \right) d\ell + \mathcal{O}(\varepsilon^2) \\ &= -\frac{1}{2k_0} \int_{\partial C_1} u_1 \frac{\partial \overline{u}_0}{\partial n} \, d\ell + \mathcal{O}(\varepsilon^2), \end{aligned} \tag{3.12}$$

using the boundary condition (3.8).

3.5 *Further simplification*

Next, we want a representation of $\partial \overline{u}_0 / \partial n$ in terms of the values of the function u_0 on the unperturbed boundary. We represent the curve ∂C_1 as being a level curve of Φ, where

$$\Phi(r, \theta) = r - \varepsilon h(\theta). \tag{3.13}$$

The unit normal vector at each point is then given by $\widehat{\mathbf{n}} = \nabla\Phi / |\nabla\Phi|$. The gradient of Φ is

$$\nabla\Phi|_{\partial C_1} = \left[\frac{\partial \Phi}{\partial r} \widehat{\mathbf{r}} + \frac{1}{r} \frac{\partial \Phi}{\partial \theta} \widehat{\theta} \right]_{\partial C_1} = \widehat{\mathbf{r}} - \frac{\varepsilon h'(\theta)}{a} \widehat{\theta} + \mathcal{O}(\varepsilon^2),$$

and so $\widehat{\mathbf{n}}|_{\partial C_1} = \widehat{\mathbf{r}} - (\varepsilon/a) h'(\theta) \widehat{\theta} + \mathcal{O}(\varepsilon^2)$. Now

$$\left. \frac{\partial \overline{u}_0}{\partial n} \right|_{\partial C_1} = \left. \frac{\partial \overline{u}_0}{\partial r} \right|_{\partial C_1} - \frac{\varepsilon h'(\theta)}{a^2} \left. \frac{\partial \overline{u}_0}{\partial \theta} \right|_{\partial C_1} + \mathcal{O}(\varepsilon^2).$$

We can expand both partial derivatives in Taylor series about $r = a$:

$$\begin{aligned} \left. \frac{\partial \overline{u}_0}{\partial n} \right|_{\partial C_1} &= \left. \frac{\partial \overline{u}_0}{\partial r} \right|_{\partial C_0} + \varepsilon h(\theta) \left. \frac{\partial^2 \overline{u}_0}{\partial r^2} \right|_{\partial C_0} - \frac{\varepsilon h'(\theta)}{a^2} \left. \frac{\partial \overline{u}_0}{\partial \theta} \right|_{\partial C_0} + \mathcal{O}(\varepsilon^2) \\ &= \varepsilon h(\theta) \left. \frac{\partial^2 \overline{u}_0}{\partial r^2} \right|_{\partial C_0} - \frac{\varepsilon h'(\theta)}{a^2} \left. \frac{\partial \overline{u}_0}{\partial \theta} \right|_{\partial C_0} + \mathcal{O}(\varepsilon^2). \end{aligned} \tag{3.14}$$

Now we note that, due to the Helmholtz equation (3.4),

$$\frac{\partial^2 \overline{u}_0}{\partial r^2} = -k_0^2 \overline{u}_0 - \frac{1}{r}\frac{\partial \overline{u}_0}{\partial r} - \frac{1}{r^2}\frac{\partial^2 \overline{u}_0}{\partial \theta^2}. \tag{3.15}$$

We obtain

$$\left.\frac{\partial \overline{u}_0}{\partial n}\right|_{\partial C_1} = -\left.\varepsilon h(\theta) k_0^2 \overline{u}_0\right|_{\partial C_0} - \left.\frac{\varepsilon h(\theta)}{a^2}\frac{\partial^2 \overline{u}_0}{\partial \theta^2}\right|_{\partial C_0} - \left.\frac{\varepsilon h'(\theta)}{a^2}\frac{\partial \overline{u}_0}{\partial \theta}\right|_{\partial C_0} + \mathcal{O}(\varepsilon^2). \tag{3.16}$$

Noting that $u_1|_{\partial C_1} = u_0|_{\partial C_0} + \mathcal{O}(\varepsilon)$, we then substitute (3.16) into (3.12) to yield

$$\begin{aligned}\delta k &= -\frac{1}{2k_0}\int_{\partial C_0} u_0 \left(-\varepsilon h(\theta) k_0^2 \overline{u}_0 - \frac{\varepsilon h(\theta)}{a^2}\frac{\partial^2 \overline{u}_0}{\partial \theta^2} - \frac{\varepsilon h'(\theta)}{a^2}\frac{\partial \overline{u}_0}{\partial \theta}\right) d\ell + \mathcal{O}(\varepsilon^2) \\ &= \frac{\varepsilon k_0}{2}\int_{\partial C_0} \left(h(\theta)|u_0|^2 + \frac{h(\theta)}{(k_0 a)^2} u_0 \frac{\partial^2 \overline{u}_0}{\partial \theta^2} + \frac{h'(\theta)}{(k_0 a)^2} u_0 \frac{\partial \overline{u}_0}{\partial \theta}\right) d\ell + \mathcal{O}(\varepsilon^2).\end{aligned} \tag{3.17}$$

This can be evaluated if the function u_0 and its derivative on the boundary are known. Let us now expand the function u_0 on the boundary in a Fourier series, so that

$$u_0|_{\partial C_0} = \sum_{\ell=-\infty}^{\infty} \alpha_\ell e^{i\ell\theta}, \tag{3.18}$$

where the coefficients α_m are known. We will also specify that the function $h(\theta)$ which controls the perturbation can be written in a similar manner, so that

$$h(\theta) = \sum_{n=-\infty}^{\infty} h_n e^{in\theta}. \tag{3.19}$$

The expression for the perturbation δk can then be written explicitly in terms of coefficients of the above expansion. Substituting into (3.17),

$$\begin{aligned}\delta k &= \frac{\varepsilon k_0 a}{2}\int_0^{2\pi} \sum_{\ell,m,n=\infty}^{\infty} \left(1 + \frac{m^2}{(k_0 a)^2} - \frac{nm}{(k_0 a)^2}\right) \alpha_\ell h_n \overline{\alpha_m}\, e^{i(\ell+n-m)\theta} d\theta \\ &= \varepsilon \pi k_0 a \sum_{\ell,n=-\infty}^{\infty} \left(1 - \frac{(n+\ell)^2}{(k_0 a)^2} + \frac{n(n+\ell)}{(k_0 a)^2}\right) \alpha_\ell h_n \overline{\alpha_{\ell+n}}.\end{aligned} \tag{3.20}$$

Here the complex conjugate is denoted by the overline. Rearranging the series in (3.20), we obtain the formula

$$\delta k = \varepsilon \pi k_0 a \sum_{\ell,m=-\infty}^{\infty} h_{m-\ell} \alpha_\ell \overline{\alpha_m} \left(1 - \frac{\ell m}{(k_0 a)^2}\right). \tag{3.21}$$

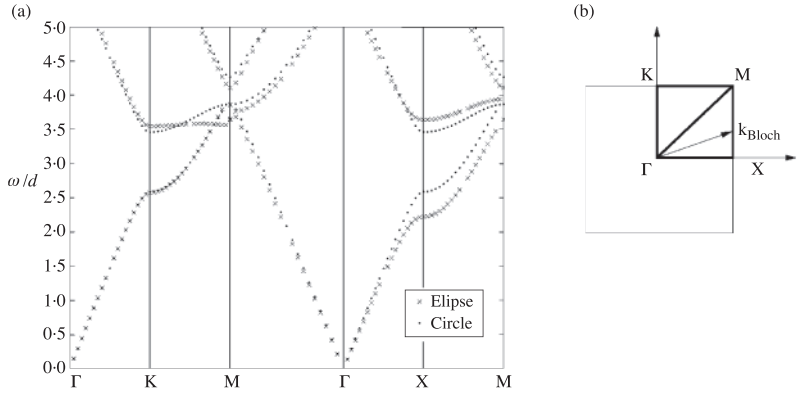

Fig. 3 (a) Dispersion curves for a TE wave moving through an array of perfectly conducting cylinders. The crosses represent the dispersion diagram for an ellipse elongated in the y-direction, with minor (x) axis $0{\cdot}20d$ and major (y) axis $0{\cdot}25d$. Also shown is the curve for the unperturbed problem, which is an array of circular cylinders of radius $0{\cdot}20d$. (b) The path traversed by $\mathbf{k}_{\text{Bloch}}$ within the first irreducible segment of the Brillouin zone

3.6 *Analysis of dispersion curves*

Using the generalized method of Rayleigh (**22**, **23**), we solved the unperturbed problem for u_0 and directly extracted the coefficients α_ℓ from the Fourier expansion of the boundary. Using the formula (3.21) we calculated the correction δk for an arbitrary perturbation.

In the numerical example, the square array has an elementary cell of the unit area and circular inclusions of radius 0·2. In Fig. 3(a) we can see the dispersion curves for an array of elliptical inclusions, whose x and y semi-axes are 0·20 and 0·25 respectively (the ellipses are oriented along the coordinate axes). A diagram showing the path taken within the Brillouin zone in the reciprocal space is included in Fig. 3(b). It is noted that, for waves travelling in the y-direction, the elliptical array behaves almost identically to an array of circular cylinders with the same cross-section in x. The difference in the dispersion relation for waves travelling in the x-direction is more apparent.

It is remarked that the algorithm presented above would work well for the case of inclusions, where transmission boundary conditions would have to be posed at the interface. The outline of this generalization is presented in Appendix B.

3.7 *Finite element modelling*

In order to compare our asymptotic approximation with independent benchmark results, we use an accurate finite element model for direct computation of eigenvalues for an elementary cell containing an elliptical void. In the text below we outline the numerical algorithm and further show that asymptotic approximation agrees well with the numerical finite element model within the range of frequencies chosen for our analysis. Let us reformulate (3.1) as

$$-\nabla \cdot (\nabla\, u) = k^2 u \text{ in } Y \setminus \bar{C} \quad \text{with} \quad \partial u/\partial n = 0 \text{ on } \partial C, \tag{3.22}$$

where C is the metallic inclusion and $Y =]0;1[^2$ denotes the elementary cell of the previous section (for the sake of simplicity, we take $d = 1$ in this section). As for the weak formulation, the homogeneous Neumann boundary condition for u on the metallic boundary is naturally fulfilled and one just has to exclude $\bar{C}$ from the basic cell Y:

$$\mathcal{R}(u,u') = \int_{Y\setminus\bar{C}} \nabla u \cdot \nabla\overline{u'}\,dx\,dy - k_0^2 \int_{Y\setminus\bar{C}} u\overline{u'}\,dx\,dy.$$

Existence and uniqueness of the solution is ensured by the Lax–Milgram lemma (see (**24**, Chapter 8)) applied to the bilinear form $\mathcal{R}(\cdot,\cdot)$ which is continuous and coercive on $H^1_\sharp(\mathbf{k}_{\text{Bloch}}, Y)\times H^1_\sharp(\mathbf{k}_{\text{Bloch}}, Y)$. Here $H^1_\sharp(\mathbf{k}_{\text{Bloch}}, Y)$ denotes the Hilbert space

$$H^1_\sharp(\mathbf{k}_{\text{Bloch}}, Y) = \left\{u \in H^1_{\text{loc}}(\mathbb{R}^2,\mathbb{C}),\ u \text{ is } (\mathbf{k}_{\text{Bloch}}, Y)\text{-periodic}\right\} \tag{3.23}$$

of $(\mathbf{k}_{\text{Bloch}}, Y)$-periodic functions (that satisfy (3.2)) which are square integrable on every compact subset of $\mathbb{R}^2$, with values in $\mathbb{C}$ and with locally square integrable gradients.

The discrete formulation is set up with nodal elements (first-order triangular elements where the unknowns are the values of the scalar field on the tips of the triangles and the interpolated field is piecewise linear on the triangles). In order to find Bloch modes with the finite element method, some changes have to be performed with respect to classical boundary-value problems that will be named *discrete Bloch conditions* (**25, 26**). A scalar discrete field $U(x,y)$ on the square cell Y with Bloch conditions relates the left and the right sides. The set of nodes is separated into three subsets: the nodes on the left (with $x = 0$), corresponding to the column vector of unknowns $\mathbf{u_l}$; the nodes on the right (with $x = 1$), corresponding to the column vector of unknowns $\mathbf{u_r}$; and the internal nodes (with $0 < x < 1$), corresponding to the column vector of unknowns $\mathbf{u}$. One has the following structure for the matrix problem (corresponding in fact to natural boundary conditions, namely, Neumann homogeneous boundary conditions):

$$\mathbf{A}\begin{pmatrix}\mathbf{u}\\ \mathbf{u_l}\\ \mathbf{u_r}\end{pmatrix} = \mathbf{b}, \tag{3.24}$$

where $\mathbf{A}$ is the (square Hermitian) matrix of the system and $\mathbf{b}$ is a column vector. The solution to be approximated by the numerical method is a discrete Bloch function $U(x,y) = U_\sharp(x,y)\ \exp\{i(k^x_{\text{Bloch}}x + k^y_{\text{Bloch}}y)\}$, $U_\sharp$ being Y-periodic and in particular $U_\sharp(x+1,y) = U_\sharp(x,y)$. Therefore,

$$U(1,y) = U_\sharp(1,y)\ \exp\{i(k^x_{\text{Bloch}} + k^y_{\text{Bloch}}y)\} = U(0,y)\ \exp(ik^x_{\text{Bloch}}) \tag{3.25}$$

and the relation between the left and the right side is

$$\mathbf{u_r} = \mathbf{u_l}\ \exp(ik^x_{\text{Bloch}}). \tag{3.26}$$

Consequently, the set of unknowns can be expressed via the reduced set $\mathbf{u}$ and $\mathbf{u_l}$,

$$\begin{pmatrix}\mathbf{u}\\ \mathbf{u_l}\\ \mathbf{u_r}\end{pmatrix} = \mathbf{P}\begin{pmatrix}\mathbf{u}\\ \mathbf{u_l}\end{pmatrix} \quad \text{with} \quad \mathbf{P} = \begin{pmatrix}\mathbf{I} & \mathbf{0}\\ \mathbf{0} & \mathbf{I}\\ \mathbf{0} & \mathbf{I}\ \exp(ik^x_{\text{Bloch}})\end{pmatrix}, \tag{3.27}$$

where **I** and **0** are identity and null matrices respectively with suitable dimensions. The finite element equations related to the eliminated nodes have now to be taken into account. Thanks to periodicity of the structure, the Bloch–Floquet conditions should be maintained on the boundary of the basic cell. Therefore their contributions (the equations corresponding to $\mathbf{u_r}$) must be added to the equations corresponding to $\mathbf{u_l}$ with the correct phase factor $\exp(-ik^x_{\mathrm{Bloch}})$. This amounts to multiplying the matrix system by $\mathbf{P}^*$, the Hermitian conjugate of **P**. Finally, the linear system to be solved is

$$\mathbf{P}^*\mathbf{A}\mathbf{P}\begin{pmatrix}\mathbf{u}\\ \mathbf{u_l}\end{pmatrix} = \mathbf{P}^*\mathbf{b}, \tag{3.28}$$

where it is worth noting that the matrix is still Hermitian, which is important for numerical computation. Now a generalized eigenvalue problem (with natural boundary conditions) $\mathbf{Au} = \lambda\mathbf{Bu}$ is transformed to an eigenvalue problem with Bloch–Floquet boundary conditions according to $\mathbf{P}^*\mathbf{APu}' = \lambda\mathbf{P}^*\mathbf{BPu}'$. Such problems involving large sparse Hermitian matrices can be solved using the Lanczos algorithm, which gives the largest eigenvalues (**27**). Physically we are in fact interested in the smallest eigenvalues and therefore $\mathbf{A}^{-1}$, the inverse of **A**, instead of **A** itself must be used in the iterations. Of course, the inverse is never computed explicitly but the matrix-vector products are replaced by system solutions thanks to a Generalized Minimal Residual (GMRES) method (**27**). It is therefore obvious that the numerical efficiency of the process relies strongly on Krylov subspace techniques and the Arnoldi iteration algorithm (**28**). The practical implementation of the model has been performed with the GETDP software (**29**).

3.8 *Comparison of analytical and numerical algorithms*

In Fig. 4 we can see the dispersion curves for an array of elliptical inclusions, with major and minor axes $0{\cdot}2d$ and $0{\cdot}3d$ respectively. Here we have compared the results with the finite element calculation. One can see that the asymptotic formula gives quite good results even when the perturbation is no longer small: in this case, $\varepsilon = 0{\cdot}5$. In the case when the eccentricity is higher (for example, elongated ellipses of major and minor axes $0{\cdot}1d$ and $0{\cdot}4d$), we have numerically checked that the asymptotic approximation fails. It is also apparent on Fig. 4 that the asymptotic formula breaks down for higher values of ω. For higher frequencies the second-order approximation (involving terms of order ε^2) would be required to obtain an accurate solution.

In the next section, we develop further the concept of mutual interaction between elements of the periodic structure. Rather than assuming that an elementary cell includes just a single void/inclusion, we look at the case of a macro-cell containing a defect (or several defects). It is observed in this case that the system may exhibit localization of eigenfields in a neighbourhood of the defect and this in turn contributes towards the coupling phenomenon.

4. Photoelastic effects. Localized modes

Finally, we would like to analyse the coupling between electromagnetic and elastic waves where the photoelastic effect occurs in periodic structures with defects. One important feature of such structures is that they possess localized defect modes for certain frequencies of elastic vibrations. As explained below, the optical properties of photoelastic material change significantly within the regions subject to large dilatation. Our model enables us to give accurate estimates for such frequencies and to describe the localized defect states.

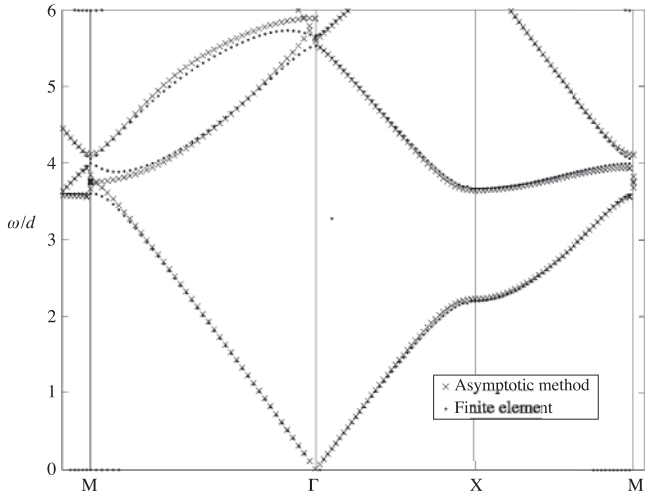

Fig. 4 Sample dispersion curves for a TE wave moving through an array of elliptical voids, with major and minor axes $0{\cdot}2d$ and $0{\cdot}3d$. A comparison with the results from a finite element method is shown. This diagram illustrates good agreement between the numerical and asymptotic results: it is noted that only the dispersion curves corresponding to the contour ΓXK are shown here

4.1 *Finite element modelling*

For an isotropic medium the relation between stress and strain is written down in the form

$$\begin{pmatrix} \sigma_{11} \\ \sigma_{22} \\ \sqrt{2}\sigma_{12} \end{pmatrix} = \mathbf{A} \begin{pmatrix} e_{11} \\ e_{22} \\ \sqrt{2}e_{12} \end{pmatrix}, \tag{4.1}$$

where $e_{ij} = (\partial u_i/\partial x_j + \partial u_j/\partial u_i)/2$,

$$\mathbf{A} = \frac{E}{(1+\nu)(1-\nu)} \begin{pmatrix} 1-\nu & \nu & 0 \\ \nu & 1-\nu & 0 \\ 0 & 0 & (1-2\nu)/\sqrt{2} \end{pmatrix}, \tag{4.2}$$

$E = \mu(3\lambda + 2\mu)/(\lambda + \mu)$ and $\nu = \lambda/[2(\lambda + \mu)]$. Hence, the equations of motion yield

$$\sigma_{ij,j} + \rho\omega^2 u_j = 0. \tag{4.3}$$

Introducing the matrix differential operator

$$\mathbf{D} = \begin{pmatrix} \partial/\partial x_1 & 0 & 2^{-1/2}\partial/\partial x_2 \\ 0 & \partial/\partial x_2 & 2^{-1/2}\partial/\partial x_1 \end{pmatrix} \tag{4.4}$$

we note that

$$\begin{pmatrix} e_{11} \\ e_{22} \\ \sqrt{2}\,e_{12} \end{pmatrix} = \mathbf{D}^{\mathbf{T}} \begin{pmatrix} u_1 \\ u_2 \end{pmatrix}. \tag{4.5}$$

We obtain the self-adjoint form

$$\mathbf{DAD^T}\begin{pmatrix} u_1 \\ u_2 \end{pmatrix} + \rho\omega^2 \begin{pmatrix} u_1 \\ u_2 \end{pmatrix} = 0. \tag{4.6}$$

As for the weak formulation, the traction free boundary conditions on the boundary of the void are naturally fulfilled and one just has to exclude C from the basic cell Y:

$$\mathcal{R}(u, u') = \int_{Y\setminus\bar{C}} \left(-\mathbf{AD^T u} \cdot \mathbf{D^T}\bar{\mathbf{u}} + \rho\omega^2 \mathbf{u} \cdot \bar{\mathbf{u}}\right) dx\, dy. \tag{4.7}$$

Existence and uniqueness of the solution is ensured by the Lax–Milgram lemma applied to the bilinear form $\mathcal{R}(\cdot,\cdot)$ which is continuous and coercive on $[H^1_\sharp(\mathbf{k}_{\text{Bloch}}, Y)]^2 \times [H^1_\sharp(\mathbf{k}_{\text{Bloch}}, Y)]^2$. Here $[H^1_\sharp(\mathbf{k}_{\text{Bloch}}, Y)]^2$ denotes the Hilbert space

$$[H^1_\sharp(\mathbf{k}_{\text{Bloch}}, Y)]^2 = \left\{u \in H^1_{\text{loc}}(\mathbb{R}^2, \mathbb{C}^2), \quad u \text{ is } (\mathbf{k}_{\text{Bloch}}, Y)\text{-periodic}\right\} \tag{4.8}$$

of $(\mathbf{k}_{\text{Bloch}}, Y)$-periodic functions (that satisfy (3.2)) which are square integrable on every compact subset of $\mathbb{R}^2$, with vector values in $\mathbb{C}^2$ and with locally square integrable gradients. The discrete formulation is set up with nodal elements (see section 3.7). Our finite element formulation has been implemented in the software FEMLAB with a macro-cell containing 48 voids. This allows us to model a defect within a macro-cell in a periodic structure. In Fig. 5, we show a localized pressure mode at the normalized radian frequency[†] $\omega = 7{\cdot}7$ placed within the stop gap corresponding to the periodic structure with periodic defects (Fig. 6). The existence of this stop band is not predicted by the spectral problem associated with the corresponding periodic structure without defect (**23**). The mechanism leading to the appearance of this high-frequency localized pressure mode is new. It is induced by the multi-scale geometry of the structure. The defects are indeed arranged on an array of larger period than that of the lattice (which corresponds to the size of the macro-cell). Addition or removal of other defects within the macro-cell will change the number of scales associated with the structure, and hence the nature of the Bloch spectrum.

4.2 *Photoelastic interaction*

Brillouin predicted in 1922 the diffraction of light by an acoustically perturbed medium: this is the so-called Brillouin scattering. When an elastic wave propagates in a medium, there is an associated strain field which results in a change of the index of refraction. This is referred to as the photoelastic effect. The photoelastic effect in a material couples the mechanical strain tensor e_{kl} to the optical index of refraction n. This effect is described by the change in the so-called optical impermeability tensor (see, for example, (**30**, Chapter 9)),

$$\nabla^2 (n^{-2})_{ij} = p_{ijkl} e_{kl}, \quad i, j, k, l = 1, 2, \tag{4.9}$$

[†] The normalization is introduced in such a way that a frequency is divided by the shear wave speed and further multiplied by the distance between centres of neighbouring inclusions/voids within the array. The displacement eigenfield, obtained as a result of the computation, is also normalized in such a way that its L_2 norm over the macro-cell is equal to one.

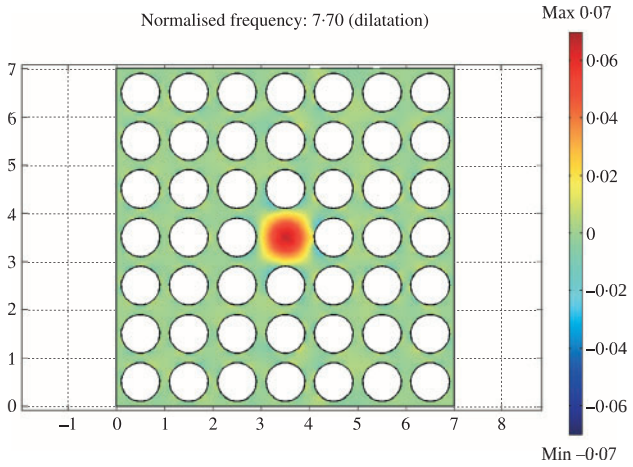

Fig. 5 Dilatation mode in a macro-cell of normalized size 7×7 with 48 voids of normalized radius 0·4 in a silica matrix. The central void has been removed to create a defect

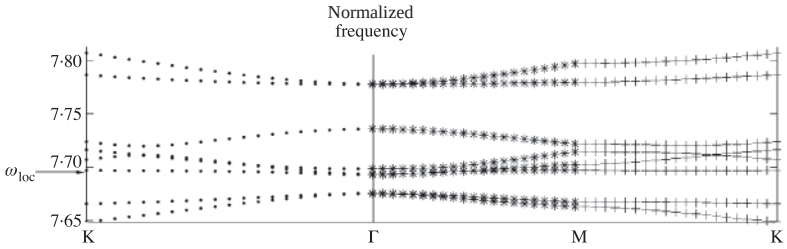

Fig. 6 Dispersion curves corresponding to in-plane elastic waves within a macro-cell shown in Fig. 5. Here, we represent the normalized frequency ω (introduced in such a way that it is divided by the distance d between centres of neighbouring voids and multiplied by the velocity of shear waves) versus the normalized modulus of Bloch vector $k_{\text{Bloch}}d$, for a normalized radius of voids 0·4. On the horizontal semi-axis we show the values of $-k_{\text{Bloch}}d$ when $\mathbf{k}_{\text{Bloch}}$ represents points of the part KΓ of the contour ΓMK. Note that here $\Gamma = (0, 0)$, M$= (0, \pi/7)$ and K$= (\pi/7, \pi/7)$

where **p** is the rank four strain-optic tensor. Thanks to the symmetry of the optical impermeability and strain tensors, we can rewrite (4.9) in contracted form

$$\nabla^2(n^{-2})_i = p_{ij}S_j, \quad i, j = 1, 2, 3, \tag{4.10}$$

where $S_1 = e_{11}$, $S_2 = e_{22}$ and $S_3 = e_{33}$.

In the case of a two-dimensional isotropic photoelastic material, $\mathbf{p}$ is given by

$$\mathbf{p} = \begin{pmatrix} p_{11} & p_{12} & 0 \\ p_{12} & p_{11} & 0 \\ 0 & 0 & (p_{11} - p_{12})/2 \end{pmatrix}. \tag{4.11}$$

We note that if $p_{11} = p_{12}$ then the contribution to shear strain is cancelled and only pressure modes are important. As an example, consider glass ($Ge_{33}Se_{55}As_{12}$) where $p_{11} = p_{12} = 0{\cdot}21$ for the wavelength $\lambda = 1{\cdot}06\,\mu$m. In the other example, for fused silica $p_{11} = 0{\cdot}121$, $p_{12} = 0{\cdot}270$ for the wavelength $\lambda = 0{\cdot}63\,\mu$m; in this case the optical properties would change within the region of localized strain, both in pressure and shear modes.

The numerical simulation was conducted for a spectral problem of two-dimensional elasticity (plane strain), with the Bloch–Floquet boundary conditions posed on the contour of a macro-cell (the elementary cell of the doubly periodic structure is shown in Fig. 5). As Fig. 5 shows, the macro-cell contains a defect, right at the centre, and in this particular case there exist eigenmodes that give a localized dilatational deformation in the region of the defect. Also, in Fig. 6, we depict the band diagram corresponding to the macro-cell of Fig. 5. This numerically demonstrates the mechanism leading to existence of a localized pressure eigenstate when we remove the central hole within the macro-cell. It is indeed clear from Fig. 6 that the eigenfrequency associated with the localized state is on the edge of the stop band shown on the dispersion diagram.

In Fig. 5 we show such a localized eigenmode corresponding to a high intensity of dilatation within a defect region in a doubly periodic array of circular voids. This diagram was constructed for fused silica and it corresponds to the zero Bloch vector which implies periodicity at the edges of the macro-cell. Compared with results of sections 2 and 3 the change in the optical properties is not small and the mechanism of localization within periodic structures with defects dominates over two remaining cases discussed earlier. It is noted that the effect of Brillouin scattering will exist for other frequencies, corresponding to non-localized eigenmodes, but the effect of coupling between the elastic and electromagnetic fields will be greatly reduced compared to the configuration shown in Fig. 5.

4.3 *Analytical estimate for the eigenfrequency corresponding to a localized mode*

The results of finite element numerical modelling presented in Fig. 5 are useful if we would like to see the shape of the region of localized dilatation; by dilatation we mean $\nabla \cdot \mathbf{u}$, where the displacement eigenfield $\mathbf{u}$ is normalized in such a way that its L_2 norm over the macro-cell is equal to unity. If we are interested in the frequency corresponding to this localized mode, an estimate can be given in a simple analytical form. Here we give an estimate of frequencies of localized axisymmetric dilatational modes. Taking into account that the displacement on the boundary of the 'defect region' is very small (the eigenmode is highly localized, as shown in Fig. 5), we consider just the defect region itself and fix its boundary. In the present example the defect region is taken as a disk of radius $a = 0{\cdot}1$. The dispacement field $\mathbf{U}(\mathbf{x}) = \mathbf{U}(x, y)$ satisfies the Navier equations

$$(\lambda + 2\mu)\nabla\nabla \cdot \mathbf{U}(\mathbf{x}) - \mu\nabla \times \nabla \times \mathbf{U}(\mathbf{x}) + \rho\omega^2\mathbf{U}(\mathbf{x}) = \mathbf{0}, \quad |\mathbf{x}| < a, \tag{4.12}$$

where ω is the radian frequency of vibration. Now, we assume that $\mathbf{U}|_{r=a} = 0$ and $\mathbf{U} = f(r, \omega)\,\mathbf{x}/|\mathbf{x}|$; U is bounded at $r = 0$. Noting that $\mathbf{U}$ is irrotational, it follows that

$$(\lambda + 2\mu)\nabla\nabla \cdot \mathbf{U}(\mathbf{x}) + \rho\omega^2\mathbf{U}(\mathbf{x}) = \mathbf{0}, \quad r = |\mathbf{x}| < a. \tag{4.13}$$

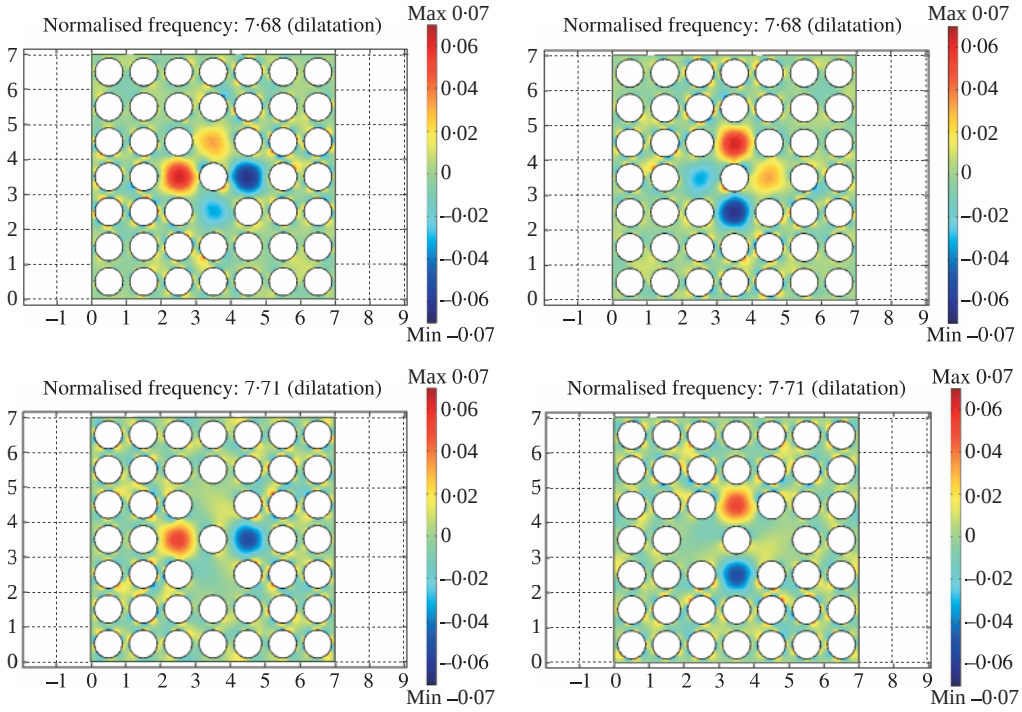

Fig. 7 Dilatation modes in a macro-cell with 45 voids in silica. Four central voids have been removed to create quadrupole core defect

Finally, by writing $\mathbf{U} = \nabla\phi$, we deduce that ϕ is a solution of the Helmhlotz equation

$$\nabla^2\phi(r) + (\omega/v)^2\phi(r) = 0, \quad r < a, \tag{4.14}$$

where $v = \sqrt{(\lambda + 2\mu)/\rho}$. Also, ϕ satisfies a Neumann condition $\partial\phi/\partial r = 0$ on the circular boundary $r = a$. Hence, it follows that $\phi = J_0(r\omega/v)$, and

$$(\omega/v)J_0'(\omega a/v) = 0. \tag{4.15}$$

Solutions of this equation approximate eigenfrequencies of the localized pressure modes (see Fig. 5). If we take a normalized radius $a = 1{\cdot}0$ (diameter of the defect) and normalized Lamé coefficients $\lambda = 2{\cdot}3$, $\mu = 1{\cdot}0$ and density $\rho = 1{\cdot}0$ (the corresponding Poisson ratio is close to 0·35 which is the same as for silica), then the estimate for the normalized frequency is $\omega = 8$ whereas the finite element software provides $\omega = 7{\cdot}7$, and indeed the asymptotic approximation is reasonable.

5. Concluding remarks and further developments

In this paper, we have shown that the mechanism which dominates the interactions between elastic and electromagnetic waves is associated with localized defect modes in photoelastic materials. We

have also given a simple illustration for a single defect and have shown an analytical estimate for the frequency corresponding to this localized mode. This idea allows for substantial development. For example, our model enables us to describe multiple localized modes of different types of symmetry, as shown in Fig. 7. Assuming that the structure shown in Fig. 7 represents a cross-section of a photonic crystal fibre, we can change the properties of the transmitted optical signal by initiating localized elastic vibrations at certain frequencies. Hence, this kind of structure can be used in the design of optical switches and this study certainly has a wide range of practical applications.

We have demonstrated an asymptotic approach described in sections 2 and 3 to evaluate the effect of coupling between elastic and electromagnetic waves in thin-walled structures and doubly periodic structures. In both cases, the effect was small. Nevertheless for a doubly periodic array of quasi-circular voids we have derived a useful analytical representation, which can be used to extend the Rayleigh method to non-circular geometries. In addition, these analytical results can be used in optimization algorithms to find an optimal shape of voids and consequently maximize the width of the stop bands on the dispersion diagrams.

Acknowledgments

We would like to thank Professor G. J. Rodin and Professor P. St J. Russell for their time and valuable discussions. This work was partly undertaken while the first author was funded by the EPSRC research grant (GR/M93994) and Professor A. Nicolet was visiting Liverpool University. Finally, we would like to thank the referees for their constructive and valuable comments and suggestions.

References

1. L. Brillouin, *La Théorie des Quanta et l'Atome de Bohr* (Presses Universitaires de France, Paris 1923).
2. P. Debye, *Methods to Determine the Electrical and Geometrical Structure of Molecules*, Nobel Lectures, Chemistry 1922–1941 (Elsevier, Amsterdam 1941) 383–401.
3. P. St J. Russell, E. Marin, A. Diez, S. Guenneau and A. B. Movchan, Sonic band-gaps in PCF preforms: enhancing the interaction of sound and light, *Optics Express* **11** (2003) 2555–2560.
4. J. Sapriel, *Acousto-Optics* (Wiley, New York 1979).
5. C. Kittel, *Introduction to Solid State Physics*, 7th edn (Wiley, New York 1996).
6. D. F. Nelson, *Electric, Optic and Acoustic Interactions in Dielectrics* (Wiley, New York 1979).
7. E. I. Gordon, A review of acousto-optical deflection and modulation devices, *Proc. IEEE* **54** (1967) 1391–1400.
8. R. Adler, Interaction between light and sound, *IEEE Spectrum* **4** (1967) 42–48.
9. J. P. Wolfe, *Imaging Phonons. Acoustic Wave Propagation in Solids* (Cambridge University Press, Cambridge 1998).
10. T. A. Birks, P. J. Roberts, P. St J. Russell, D. M. Atkin and T. J. Shepherd, Full 2-D photonic bandgaps in silica/air structures, *Electronic Letters* **31** (1995) 1941–1942.
11. J. C. Knight, J. Broeng, T. A. Birks and P. St J. Russell, Photonic band gap guidance in optical fibers, *Science* **282** (1998) 1476–1478.
12. C. G. Poulton, S. Guenneau, A. B. Movchan and A. Nicolet, Transverse propagating waves in perturbed periodic structures, *Asymptotics, Singularities and Homogenisation in Problems in Mechanics* (ed. A. B. Movchan; Kluwer, Dordrecht 2003) 147–158.

13. G. A. Maugin, *Continuum Mechanics of Electromagnetic Solids* (North–Holland, Amsterdam 1988).
14. L. D. Landau, E. M. Lifshitz and L. P. Pitaevskii, *Electrodynamics of Continuous Media* (Butterworth–Heinemann, New York 1984).
15. U. Müller and L. Bühler, *Magnetofluiddynamics in Channels and Containers* (Springer, Berlin 2001).
16. S. Briguglio, G. Vlad, F. Zonca and G. Fogaccia, Nonlinear saturation of shear Alfven modes and self-consistent energetic ion transport in burning plasmas with advanced tokamak equilibria, *Phys. Lett.* A **302** (2002) 308–312.
17. K. M. Leung and Y. F. Liu, Full vector wave calculation of photonic band structures in face-centred cubic dielectric media, *Phys. Rev. Lett.* **65** (1990) 2646–2649.
18. N. A. Nicorovici, R. C. McPhedran and B. Ke-Da, Propagation of electromagnetic waves in periodic lattices of spheres. Green's function and lattice sums, *Phys. Rev.* E **51** (1995) 690–702.
19. J. B. Pendry, Calculating photonic band structure, *J. Phys. Condensed Matter* **8** (1996) 1085–1108.
20. S. Agmon, A. Douglis and L. Nirenberg, Estimates near the boundary for solutions of elliptic partial differential equations satisfying general boundary conditions, I, *Comm. Pure Appl. Math.* **12** (1959) 623–727.
21. ——, —— and ——, Estimates near the boundary for solutions of elliptic partial differential equations satisfying general boundary conditions, II, *ibid.* **17** (1964) 35–92.
22. N. A. Nicorovici, R. C. McPhedran and L. C. Botten, Photonic band gaps for arrays of perfectly conducting cylinders, *Phys. Rev.* E **52** (1995) 1135–1145.
23. C. G. Poulton, A. B. Movchan, R. C. McPhedran, N. A. Nicorovici and Y. A. Antipov, Eigenvalue problems for doubly periodic elastic structures and phononic band gaps, *Proc. R. Soc.* A **456** (2000) 2543–2559.
24. H. Brezis, *Analyse Fonctionnelle* (Masson, Paris 1983).
25. Ph. Langlet, A.-C. Hladky-Hennion and J.-N. Decarpigny, Analysis of the propagation of plane acoustic waves in passive periodic materials using the finite element method, *J. Acoust. Soc. Amer.* **98** (1995) 2792–2800.
26. A. Nicolet, S. Guenneau, C. Geuzaine and F. Zolla, Modeling of electromagnetic waves in periodic media with finite elements, *J. Comp. Appl. Math.* **168** (2004) 321–329.
27. B. Meys, Ph.D. Thesis. Université de Liège (1999).
28. L. N. Trefethen and D. Bau III, *Numerical Linear Algebra* (SIAM, Philadelphia 1997).
29. P. Dular, C. Geuzaine, F. Henrotte and W. Legros, A general environment for the treatment of discrete problems and its application to the finite element method, *IEEE Trans. on Magnetics* **34** (1998) 3395–3398.
30. A. Yariv and P. Yeh, *Optical Waves in Crystals: Propagation and Control of Laser Radiation* (Wiley, New York 1984).

APPENDIX A

Asymptotic procedure for a thin body vibrating in an electromagnetic field

This Appendix gives the details of the asymptotic algorithm used in the derivation of the lower-dimensional model of section 2.

An asymptotic algorithm in the middle part of the thin region Π_ε

Introduce the scaled variable $\zeta = x_2/\varepsilon$, so that $\zeta \in (-1/2, 1/2)$ within Π_ε; $\partial/\partial x_2 = \varepsilon^{-1}\partial/\partial\zeta$. The fields $\mathbf{E}$, $\mathbf{H}$ and $\mathbf{u}$ are approximated in the form

$$\begin{aligned}\mathbf{E} &\sim \mathbf{E}^{(0)}(x_1,\zeta,t) + \varepsilon\mathbf{E}^{(1)}(x_1,\zeta,t) + \varepsilon^2\mathbf{E}^{(2)}(x_1,\zeta,t),\\ \mathbf{H} &\sim \mathbf{H}^{(0)}(x_1,\zeta,t) + \varepsilon\mathbf{H}^{(1)}(x_1,\zeta,t) + \varepsilon^2\mathbf{H}^{(2)}(x_1,\zeta,t),\\ \mathbf{u} &\sim \mathbf{u}^{(0)}(x_1,\zeta,t) + \varepsilon\mathbf{u}^{(1)}(x_1,\zeta,t) + \varepsilon^2\mathbf{u}^{(2)}(x_1,\zeta,t).\end{aligned}$$

It follows from (2.2) that

$$\frac{\partial}{\partial\zeta}\mathbf{E}^{(j)} + \frac{\partial}{\partial x_1}\mathbf{E}^{(j-1)} = 0 \quad \text{and} \quad \frac{\partial}{\partial\zeta}\mathbf{H}^{(j)} + \frac{\partial}{\partial x_1}\mathbf{H}^{(j-1)} = 0, \tag{A.1}$$

where the quantities with negative indices are replaced by zero; hence

$$\frac{\partial}{\partial\zeta}\begin{pmatrix}\mathbf{E}^{(0)}\\ \mathbf{H}^{(0)}\end{pmatrix} = 0 \ \text{ as } \zeta \in (-1/2, 1/2), \tag{A.2}$$

which yields that $\mathbf{E}^{(0)}$ and $\mathbf{H}^{(0)}$ are ζ-independent. Taking into account the boundary condition (2.8) we deduce $\mathbf{E}^{(0)} = \mathbf{E}^{(e)}|_{x_2=0}$ and $\mathbf{H}^{(0)} = \mathbf{H}^{(e)}|_{x_2=0}$. It will be shown that only $\mathbf{E}^{(0)}$ and $\mathbf{H}^{(0)}$ will be required in the equations of motion for the displacement components. Next, consider the system of Navier equations (see (2.6))

$$\mathbf{L}(\partial/\partial x, \partial/\partial\zeta)\mathbf{u} + \mu_0\sigma\mathbf{E}\times\mathbf{H} + \mu_0^2\sigma(\dot{\mathbf{u}}\times\mathbf{H})\times\mathbf{H} = \rho\ddot{\mathbf{u}}, \tag{A.3}$$

where the differential operator $\mathbf{L}$ is given by

$$\mathbf{L}\mathbf{u} = \varepsilon^{-2}\begin{pmatrix}\mu & 0\\ 0 & 2\mu+\lambda\end{pmatrix}\frac{\partial^2\mathbf{u}}{\partial\zeta^2} + \varepsilon^{-1}\begin{pmatrix}0 & \lambda+\mu\\ \lambda+\mu & 0\end{pmatrix}\frac{\partial^2\mathbf{u}}{\partial x_1\partial\zeta} + \begin{pmatrix}2\mu+\lambda & 0\\ 0 & \mu\end{pmatrix}\frac{\partial^2\mathbf{u}}{\partial x^2}. \tag{A.4}$$

The traction boundary condition (2.9) at the upper and lower parts of the boundary $\partial\Pi_\varepsilon$ has the matrix representation $\mathbf{T}(\partial/\partial x_1, \partial/\partial\zeta)\mathbf{u}|_{\zeta=\pm1/2} = 0$, where

$$\mathbf{T}\left(\frac{\partial}{\partial x_1}, \frac{\partial}{\partial\zeta}\right)\mathbf{u} = \varepsilon^{-1}\begin{pmatrix}\mu & 0\\ 0 & 2\mu+\lambda\end{pmatrix}\frac{\partial\mathbf{u}}{\partial\zeta} + \begin{pmatrix}0 & \mu\\ \lambda & 0\end{pmatrix}\frac{\partial\mathbf{u}}{\partial x_1}. \tag{A.5}$$

Model problems on the scaled cross-section

For the vector function $\mathbf{u}^{(0)}$ we obtain (by collecting terms of order $O(\varepsilon^{-2})$ in (A.4) and terms of order $\mathcal{O}(\varepsilon^{-1})$in (A.5))

$$(\partial^2/\partial\zeta^2)\mathbf{u}^{(0)} = 0, \quad |\zeta| < \tfrac{1}{2}, \quad \text{with} \quad (\partial/\partial\zeta)\mathbf{u}^{(0)}|_{\zeta=\pm1/2} = 0. \tag{A.6}$$

Hence $\mathbf{u}^{(0)} = \mathbf{u}^{(0)}(x_1, t)$ (it is ζ-independent). In a similar way, it is derived that the vector function $\mathbf{u}^{(1)}$ satisfies the following model problem on the scaled cross-section:

$$\frac{\partial^2\mathbf{u}^{(1)}}{\partial\zeta^2} = 0, \quad |\zeta| < \tfrac{1}{2}, \quad \text{with} \quad \begin{pmatrix}\mu & 0\\ 0 & 2\mu+\lambda\end{pmatrix}\frac{\partial\mathbf{u}^{(1)}}{\partial\zeta}\bigg|_{\zeta=\pm1/2} = -\begin{pmatrix}0 & \mu\\ \lambda & 0\end{pmatrix}\frac{\partial\mathbf{u}^{(0)}}{\partial x_1}. \tag{A.7}$$

The constant of integration is chosen in such a way that the solution of (A.7) possesses a zero average across the interval $(-1/2, 1/2)$:

$$\mathbf{u}^{(1)} = -\zeta\begin{pmatrix}0 & 1\\ \lambda(2\mu+\lambda)^{-1} & 0\end{pmatrix}\frac{\partial}{\partial\zeta}\mathbf{u}^{(0)}. \tag{A.8}$$

The next model problem is for the function $\mathbf{u}^{(2)}$:

$$\frac{\partial^2 \mathbf{u}^{(2)}}{\partial \zeta^2} = -\begin{pmatrix} \mu^{-1} & 0 \\ 0 & (2\mu+\lambda)^{-1} \end{pmatrix} \Big\{ \begin{pmatrix} 2\mu+\lambda & 0 \\ 0 & \mu \end{pmatrix} \frac{\partial^2 \mathbf{u}^{(0)}}{\partial x_1^2} - (\lambda+\mu) \begin{pmatrix} \lambda(2\mu+\lambda)^{-1} & 0 \\ 0 & 1 \end{pmatrix} \frac{\partial^2 \mathbf{u}^{(0)}}{\partial x_1^2} + \mu_0^2 \sigma \Big\{ ((H_1^{(0)})^2 + (H_2^{(0)})^2) \dot{\mathbf{u}}^{(0)} - (\dot{u}_1^{(0)} H_1^{(0)} + \dot{u}_2^{(0)} H_2^{(0)}) \mathbf{H}^{(0)} \Big\} + \mu_0 \sigma \mathbf{E}^{(0)} \times \mathbf{H}^{(0)} - \rho \ddot{\mathbf{u}}^{(0)} \Big\} \quad \text{(A.9)}$$

for $\zeta \in (-1/2, 1/2)$, with

$$\left. \frac{\partial \mathbf{u}^{(2)}}{\partial \zeta} \right|_{\zeta = \pm 1/2} = \pm \frac{1}{2} \begin{pmatrix} \mu^{-1} & 0 \\ 0 & (2\mu+\lambda)^{-1} \end{pmatrix} \begin{pmatrix} \mu\lambda(2\mu+\lambda)^{-1} & 0 \\ 0 & \lambda \end{pmatrix} \frac{\partial^2 \mathbf{u}^{(0)}}{\partial x_1^2}. \quad \text{(A.10)}$$

The solvability condition of the above problem takes the form (2.10).

APPENDIX B

Perturbation for the TE mode, dielectric case

We now look at the case for which the solution is permitted to exist in two distinct regions. This corresponds to the dielectric case in the context of electromagnetism, that is, when the central inclusion has a refractive index n rather than being perfectly conducting as in section 3.

We assume that the unperturbed problem satisfies the following differential equations:

$$(\nabla^2 + k_0^2) u_0 = 0 \quad \text{in } \Omega_0 \quad \text{and} \quad (\nabla^2 + n^2 k_0^2) u_0^i = 0 \quad \text{in } C_0.$$

On the boundary of the inclusion we specify the conditions

$$u_0|_{\partial C_0} = u_0^i\Big|_{\partial C_0} \quad \text{and} \quad \left.\frac{\partial u_0}{\partial n}\right|_{\partial C_0} = \left.\frac{1}{n^2}\frac{\partial u_0^i}{\partial n}\right|_{\partial C_0},$$

where n is the relative refractive index between the central region and the surrounding matrix material. The boundary conditions are appropriate for a transverse electric wave in the context of electromagnetism; in this case the potential u_0 represents the out-of-plane component of the magnetic field. As in section 3 the periodicity of the problem requires that the Bloch–Floquet condition (3.2) be satisfied throughout the unit cell as shown in Fig. 1. Also, we normalize the energy stored in the field, so that

$$\int_{C_0} |u_0^i|^2 dA + \int_{\Omega_0} |u_0|^2 dA = 1. \quad \text{(B.1)}$$

We now perturb the boundary of the central inclusion so that $\partial C_0 \to \partial C_1$ as described by (3.6) and Fig. 2. The perturbed fields then satisfy the differential equations

$$(\nabla^2 + k_1^2) u_1 = 0 \quad \text{in } \Omega_1 \quad \text{and} \quad (\nabla^2 + n^2 k_1^2) u_1^i = 0 \quad \text{in } C_1,$$

while on the perturbed boundary we have the conditions

$$u_1|_{\partial C_1} = u_1^i\Big|_{\partial C_1} \quad \text{and} \quad \left.\frac{\partial u_1}{\partial n}\right|_{\partial C_1} = \left.\frac{1}{n^2}\frac{\partial u_1^i}{\partial n}\right|_{\partial C_1}.$$

We also require that the perturbed field u_1 satisfy the quasiperiodicity condition (3.2).

We apply Green's theorem in Ω_1 to u_1 and $\overline{u}_0$. Taking into account the quasiperiodicity of the fields, we deduce that the integral around the outer boundary B is zero. Rearranging slightly we obtain

$$(k_0^2 - k_1^2) \int_{C_1} u_1^i \overline{u}_0^i \, dA = \frac{1}{n^2} \int_{\partial C_1} \left(\overline{u}_0^i \frac{\partial u_1^i}{\partial n} - u_1^i \frac{\partial \overline{u}_0^i}{\partial n} \right) d\ell. \quad \text{(B.2)}$$

Adding (B.2) to (3.10) we obtain

$$(k_0^2 - k_1^2)\left[\int_{\Omega_1} u_1 \overline{u}_0 \, dA + \int_{C_1} u_1^i \overline{u}_0^i \, dA\right] = \int_{\partial C_1} \left[u_1 \left(\frac{\partial \overline{u}_0}{\partial n} - \frac{1}{n^2}\frac{\partial \overline{u}_0^i}{\partial n}\right) - \frac{\partial u_1}{\partial n}(\overline{u}_0 - \overline{u}_0^i)\right] d\ell. \quad \text{(B.3)}$$

We assume that the perturbation of the boundary is regular in character, so that $k_1 = k_0 + \mathcal{O}(\varepsilon)$,

$$\left.\begin{array}{c} u_1 = u_0 + \mathcal{O}(\varepsilon) \\ \partial u_1/\partial n = \partial u_0/\partial n + \mathcal{O}(\varepsilon) \end{array}\right\} \quad \text{in } \Omega_1 \quad \text{and} \quad \left.\begin{array}{c} u_1^i = u_0^i + \mathcal{O}(\varepsilon) \\ \partial u_1^i/\partial n = \partial u_0^i/\partial n + \mathcal{O}(\varepsilon) \end{array}\right\} \quad \text{in } C_1,$$

Here we have assumed that u_0^i can be analytically extended into the region C_1. This is equivalent to the assumption that the perturbed boundary does not exceed the limits of the central cell.

With this in mind then, we can write (B.3) in the form

$$-2k_0\delta k\left[\int_{\Omega_1} |u_0|^2 dA + \int_{C_1} |u_0^i|^2 dA\right] = \int_{\partial C_1} \left[u_0 \left(\frac{\partial \overline{u}_0}{\partial n} - \frac{1}{n^2}\frac{\partial \overline{u}_0^i}{\partial n}\right) - \frac{\partial u_0}{\partial n}(\overline{u}_0 - \overline{u}_0^i)\right] d\ell + \mathcal{O}(\varepsilon^2). \quad \text{(B.4)}$$

The integral on the left-hand side comes from the normalization (B.1), and so

$$\delta k = -\frac{1}{k_0}\int_{\partial C_1} \left[u_0 \left(\frac{\partial \overline{u}_0}{\partial n} - \frac{1}{n^2}\frac{\partial \overline{u}_0^i}{\partial n}\right) - \frac{\partial u_0}{\partial n}(\overline{u}_0 - \overline{u}_0^i)\right] d\ell + \mathcal{O}(\varepsilon^2).$$

We can deduce that

$$\left.\frac{\partial \overline{u}_0^i}{\partial n}\right|_{\partial C_1} = \left[\frac{\partial \overline{u}_0^i}{\partial r} - n^2 k_0^2 \varepsilon h(\theta)\overline{u}_0^i - \frac{\varepsilon h(\theta)}{a}\frac{\partial \overline{u}_0^i}{\partial r} - \frac{\varepsilon h(\theta)}{a^2}\frac{\partial^2 \overline{u}_0^i}{\partial \theta^2} - \frac{\varepsilon h'(\theta)}{a^2}\frac{\partial \overline{u}_0^i}{\partial \theta}\right]\Bigg|_{\partial C_0} + \mathcal{O}(\varepsilon^2),$$

and furthermore

$$\left.\left(\frac{\partial \overline{u}_0}{\partial n} - \frac{1}{n^2}\frac{\partial \overline{u}_0^i}{\partial n}\right)\right|_{\partial C_1} = -\left[\frac{\varepsilon h(\theta)}{a^2}\left(1 - \frac{1}{n^2}\right)\frac{\partial^2 \overline{u}_0}{\partial \theta^2} + \frac{\varepsilon h'(\theta)}{a^2}\left(1 - \frac{1}{n^2}\right)\frac{\partial \overline{u}_0}{\partial \theta}\right]\Bigg|_{\partial C_0} + \mathcal{O}(\varepsilon^2).$$

We also deduce, using Taylor's expansion, that

$$\left.\left(\overline{u}_0 - \overline{u}_0^i\right)\right|_{\partial C_1} = \varepsilon h(\theta)\left.\left(\partial \overline{u}_0/\partial r - \partial \overline{u}_0^i/\partial r\right)\right|_{\partial C_0} + \mathcal{O}(\varepsilon^2).$$

Thus, substituting into (B.4), we find the perturbation to k_0 as

$$\delta k = -\frac{\varepsilon}{2k_0 a^2}\left(1 - \frac{1}{n^2}\right)\int_{\partial C_0}\left(-u_0\frac{\partial}{\partial \theta}\left(h(\theta)\frac{\partial \overline{u_0}}{\partial \theta}\right) + n^2 a^2 h(\theta)\frac{\partial u_0}{\partial r}\frac{\partial \overline{u}_0}{\partial r}\right) d\ell.$$

This gives the generalization of the asymptotic formula (3.20) to the case of dielectric inclusions with the transmission boundary conditions posed at the interface.